membrane of specific types of carcinoma cells. Specifically, the over-expression in certain epithelial carcinoma cells can be as high as a thousand fold and thus FR provides an important possible target in efficient drug therapy design. In this study, we are probing the dynamics and interactions of folate/FR receptor complexes in the plasma membrane and through each part of its endocytotic cycle at the single molecule level. We are employing single molecule fluorescence microscopy to track individual fluorophore-labeled folate molecules bound to cell surface FR. We found an average diffusion constant of D = 2e-9 cm^2/s on live human KB carcinoma cells when imaged at 30 fps. Trajectories of individual particles showed temporary stopping or confined motion. This anomalous diffusive behavior was quantified against Monte Carlo simulations of randomly diffusing particles. The frequency and duration of confinement was compared as the overall concentration of folate was incrementally increased from 1 fM to the physiological level of 1nM . The effect on the frequency and duration of single FR confinement due to cholesterol depletion, actin stabilization and actin depolymerization will be presented.

1440-Pos Board B284

The Role of Cluster Size and Protein Spatial Pattern in the Immunological Synapse

Niña C. Hartman, Wan-Chen Lin, Cheng-han Yu, Jay T. Groves.
UC-Berkeley, Berkeley, CA, USA.

During antigen recognition by T cells, signaling molecules on the T cell engage ligands on the antigen-presenting cell and organize into spatially distinctive patterns collectively known as the immunological synapse (IS). The spatial arrangement of proteins into well-defined zones within the IS is known to regulate T cell activation and signal transduction. The mechanisms by which this complex organization arises remain unclear. Here we alter the clustering state of the T cell costimulatory molecule, LFA-1, either by direct antibody crosslinking or by crosslinking its ligand, ICAM-1, displayed on the supported bilayer. Changes in receptor clustering lead to progressively more central localization of LFA-1 until it colocalizes with T cell receptors (TCR) at the center. The number of LFA-1 molecules within the resulting clusters is obtained by fluorescence correlation spectroscopy. Our results demonstrate that cluster size is a critical parameter in determining protein spatial positioning in the IS. We discuss a sorting mechanism, based on frictional coupling to the cytoskeleton, which is consistent with these observations and is, in principle, extendable to all cell surface proteins in the synapse. Furthermore, by presenting patterns of immobilized ICAM-1 within a fluid bilayer displaying the TCR ligand, peptide-loaded MHC, we investigate the importance of LFA-1 ring formation to T cell function and signaling.

1441-Pos Board B285

Multispecies Single Molecule Imaging With Quantum Dots

Christoffer Lagerholm[1], Eva Arnspang Christensen[1],
Mathias Lysemose Clausen[1], Pasad Kulatunga[2].
[1]University of Southern Denmark, Odense M, Denmark, [2]Hobart and William Smith Colleges, Geneva, NY, USA.

Quantum dots (Qdots) are fluorescent nanoparticles that have far superior signal intensity and signal stability compared to more conventional fluorescent molecules. We find that imaging with Qdots can easily be extended to the simultaneous visualization of up to four different molecular species at single molecule sensitivity and millisecond time integration. We find that this technique can easily be adapted towards studying the spatial and temporal nano-organization of various combinations of lipids and proteins in the cellular plasma membrane.

Intracellular Communication & Gap Junctions

1442-Pos Board B286

Structural And Functional Significance Of The N-terminus Of Cx26 Gap Junction Channels

Atsunori Oshima[1], Kazutoshi Tani[1], Masoud M. Toloue[2], Yoko Hiroaki[1], Amy Smock[3], Bruce J. Nicholson[2], Gina E. Sosinsky[3], Yoshinori Fujiyoshi[1].
[1]Kyoto University, Kyoto, Japan, [2]University of Texas Health Science Center at San Antonio, San Antonio, TX, USA, [3]University of California San Diego, San Diego, CA, USA.

Investigations of gap junction channels have used different and often complementary experimental approaches to elucidate the gating mechanism of these intercellular conduits. However, no consensus gating model explaining the different phenomena of voltage and chemical gating has been formulated that is consistent with all mutagenesis, dye permeation, electrophysiology and electron microscopy results.

We made several N-terminal deletion constructs to assess channel structure/function. Shorter deletions such as del2-7 and del2-8 formed gap junctions when expressed in mammalian cells while longer constructs (del2-10 and 2-11) were either much less efficient or failed to form gap junctions. For our structure analysis, a full length connexin26 (Cx26M34A) and an N-terminal deletion mutant (Cx26M34Adel2-7) were over-expressed using Sf9 insect cells. Purified proteins were reconstituted into the lipid bilayers that formed 2D crystals. The 3D maps at 10Å resolution revealed that crystals obtained from both constructs were composed of three lipid bilayers with the channels forming a $p22_12_1$ lattice. The structure of Cx26M34A clearly showed a prominent density we refer to as a ''plug'', which resides in each hemichannel pore and contacts the innermost helices of surrounding subunits at the bottom of the vestibule (Oshima *et al.*, 2007). The 3D structure of Cx26M34Adel2-7 contained a reduced plug and a partially reduced density in the cytoplasmic domain that bridges the adjacent four helix bundles, suggesting that the N-terminus of Cx26 has an important role in forming a plug. Cx26M34Adel2-7 exhibited no electrical functionality. Cx26M34A channels showed little or no dye transfer and a dramatically reduced conductance, although the voltage gating characteristics of the residual conductance were normal. Physical blockage may be one of the gating mechanism of Cx26 channels, however, this may represent only one of multiple gating configurations.

1443-Pos Board B287

Effects Of Induced Post-ischemic Phosphorylation On Action Potential Propagation In Mouse Neonatal Cardiomyocytes

Joshua Thomas[1], Chris Hunter[2], Daniel A. Appadurai[2,3], **Alonso P. Moreno**[2].
[1]Division of Cardiology, University of Utah, Salt Lake City, UT, USA, [2]CVRTI University of Utah, Salt Lake City, UT, USA, [3]Dept. of Biology, Salt Lake City, UT, USA.

Intracellular events triggered by protein phosphorylation and kinase translocation have been reported to help preventing larger cardiac tissue damage. Our objective was to determine if immediate changes in phosphorylation post-infarction, resembling clinical treatments could affect conduction velocity and further cardiac protection.

Cardiomyocytes from 0-2 day old mice pups were grown on 64 Micro-Electrode Arrays (MEAs; MES, Germany). The MEAs recorded action potential (AP) propagation produced by neonatal cardiomyocytes isolated and culture for 2 days. Myocytes were subjected to ischemia by placing a 13mm glass round cover-slip over the preparation for 45 minutes and recordings were made during and after cover-slip removal. After the ischemic event, random groups were treated with 300nM TPA to induce phosphorylation for one hour. TPA was removed and both groups were incubated for 24 hours. Following incubation cells were subjected to another ischemic event. Recordings were done after the ischemic event and again thirty minutes later. Conduction velocity (CV) was averaged from all electrodes.

Phosphorylation and kinase translocation has been known to protect cardiocytes during ischemic preconditioning. We now present conditions where phosphorylation can actually be detrimental if induced after an ischemic event. At the 24 hour point, the control group had recovered AP CV by $99 \pm 2\%$ (mean $\pm$ SE) compared to the TPA treated group which recovered to $56 \pm 8\%$. The TPA treated group then showed only an average of $14 \pm 7\%$ decrease in AP CV and AP amplitude upon administering the second ischemic event whereas the control group AP CV decreased by an average of $55\% \pm 9$. When induced early after an ischemic event, phosphorylation results protective to maintain CV but appears to become detrimental for cellular survival.

1444-Pos Board B288

Different Types of Cell-to-Cell Connections Mediated By Nanotubular Structures

Maruša Lokar[1], Peter Veranič[2], Gerhard J. Schütz[3], Julian Weghuber[4], Stefan Wieser[5], Veronika Kralj-Iglič[6], Aleš Iglič[1].
[1]Laboratory of Physics, Faculty of Electrical Egineering, University of Ljubljana, SI-1000 Ljubljana, Slovenia, [2]University of Ljubljana, Institute of cell biology, Lipiceva 2, SI-1000 Ljubljana, Slovenia, [3]Biophysics Institute, Johannes Kepler University Linz, Altenbergerstr. 69, A-4040 Linz, Austria, [4]Biophysics Institute, Johannes Kepler University Linz, Altenbergerstr. 69, A-4040 Linz, Austria, [5]Biophysics Institute, Johannes Kepler University Linz, Altenbergerstr. 69, A-4040 Linz, Austria, [6]Laboratory of Clinical Biophysics, Faculty Medicine, University of Ljubljana, SI-1000 Ljubljana, Slovenia.

Communication between cells is crucial for proper functioning of multi-cellular organisms. The recently discovered membranous tubes, named tunnelling nanotubes (TNTs), that directly bridge neighbouring cells, may offer a very specific and effective way of intercellular transport and communication. Our experiments on RT4 and T24 urothelial cell lines show that TNTs can be

divided into two types with respect to their biochemical characteristics and the nature of the process of their formation. The nanotubes of type I are shorter, more dynamic and contain actin filaments. They are formed when cells explore their surroundings in order to make contact with another cell. The nanotubes of type II are longer, more stable and have cytokeratin filaments. They are formed when two already connected cells start to move apart. On the nanotubes of both types small vesicles were found as an integral part of the nanotubes (i.e. dilatations of the nanotubes). The dilatations of type II nanotubes do not move along the nanotubes, while the nanotubes of type I have frequently dilatations (gondolas) that move along the nanotubes in both directions and are formed in different ways. We suggested theoretical models that may explain how these nanotubes are created and stabilised.

References:
Veranic P. et al. Different Types of Cell-to-Cell Connections Mediated By Nanotubular Structures, Biophys J. (2008) Jul 25. doi:10.1529/biophysj.108.131375

http://www.gap.fe.uni-lj.si/

1445-Pos Board B289

Simulation Of Particle Diffusion Across Gap Junction Channels Based On Their Pore Geometry Explains Unidirectional Fluxes

Abhijit Mondal[1,2], Daniel A. Appadurai[1,3], Osman Amhed[4], Alonso P. Moreno[1].
[1]CVRTI, University of Utah, Salt Lake City, UT, USA, [2]Dept. of Mechanical Engineering, University of Utah., Salt Lake City, UT, USA, [3]Dept. of Biotechnology, University of Utah, Salt Lake City, UT, USA, [4]Division of Cardiology, University of Utah, Salt Lake City, UT, USA.

Connexin proteins form gap junction channels that allow intercellular communication with distinct perm-selectivity properties. Mono-heteromeric and heterotypic combinations of cardiac connexin43 (Cx43) and Cx45 induce a preferential flux based on molecular size. For Lucifer Yellow or Rhodamine123, preferential flux was 3x larger from homomeric to heteromeric connexons. For heterotypic combinations, fluxes from homomeric Cx45 to homomeric Cx43 connexons were 4x larger. This favored direction was not expected. **Our objective was to use computational simulation of particle diffusion across gap junction channel pores to find if geometrical parameters can explain our in vitro permeability data.**

HeLa cells were stained with red or green dyes to differentiate expression and co-cultured on glass cover-slips for 8 hours. A Nikon epifluorescent Eclipse7000 microscope helped quantifying diffusion. Fluorescent dyes were iontophoretially injected into a single red cell surrounded by green cells. Coupling coefficient (cells touching the injected cell/touching cells with dye) was determined 3 min after.

3D geometric model of the pore was mathematically modeled combining cylinders, cones and an ellipsoid. Particle position, velocity, acceleration and force vectors were calculated after every time step (10^{-14} s), considering wall-particle and particle-particle elastic interactions, inter-particle electrostatic, Brownian and other forces. Particles' paths were recorded and those crossing the pore were counted. Without electric field, number of particles crossing increased linearly as mouth radius increased. With an electric field, number of particles crossing varied non-linearly with a maximum when radius was around 21.4 Å. **Our computer simulations predict that changes in phosphorylation, voltage or connexin recombination yield to changes in pore structure which in turn affects large molecules' permeability.**

1446-Pos Board B290

Diffusion-Sensing versus Quorum Sensing in a Model Biofilm

Utkur M. Mirsaidov[1], Jan Scrimgeour[1], Winston Timp[2], Gene Tsvid[1], Gregory L. Timp[1].
[1]Beckman Institute, University of Illinois-Urbana, Urbana, IL, USA, [2]Whitehead Institute, MIT, Boston, MA, USA.

Cell interactions through soluble signaling molecules control differentiation, immune response and other physiologically vital processes in everything from tissue to biofilms. We tested a model of a bacterial biofilm, which uses an autoinducer (AI), N-acyl-L-homoserine lactone (AHL) for signaling, to discriminate quorum-sensing (QS) and diffusion-sensing (DS). The AI induces the transcription of a set of genes that includes the gene-encoding the AI-producing enzyme, promoting a positive feed-back. We creating a synthetic biofilm using a microfluidic network, to convey cells to an assembly area where multiple, time-shared optical tweezers are used to array them. The cells are encapsulated in a 30μm×30μm×45μm volume of hydrogel mimicking an extra-cellular matrix. To extend the size, shape and constituency of the array, we then step to an adjacent location while maintaining registration with the reference array, and repeat the process as illustrated in Figure 1(a). Using this step-and-repeat method, we formed arrays of *E. coli* engineered to produce AHL, which is functionally linked to a fluorescence reporter. As shown in Fig. 1(d), the threshold to induce AI production and fluorescence depends on the number of cells and the mass-transfer, indicating that QS is a side effect of DS.

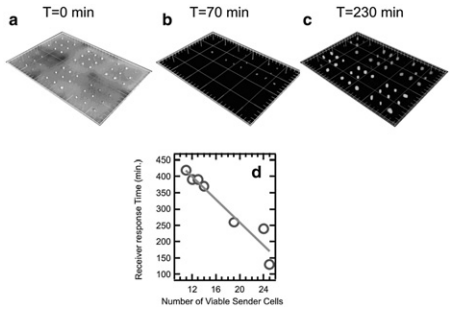

1447-Pos Board B291

Identification of Transmembrane Helix 2 (M2) as the Main Pore-Lining Helix of Connexin 43 Gap-Junctional Hemichannels (GJH)

Sung-Chang Lee[1], Seung-Hee Choi[1], Catherine F. Hamilton[1], Luis Reuss[1], R. Bryan Sutton[2], Guillermo A. Altenberg[1].
[1]Texas Tech University Health Sciences Center, Lubbock, TX, USA, [2]The University of Texas Medical Branch, Galveston, TX, USA.

GJH are connexin hexamers that dock head-to-head to form gap-junctional channels. Current GJH models are based on low-resolution structural data showing 4 transmembrane α helices per connexin monomer, with insufficient detail for helix assignment; helices have been named A, B, C and D, with B and C as pore-lining. Here, we used luminescence resonance energy transfer to calculate distances between same-position residues in diametrically-opposed monomers of purified GJH formed by functional single-cysteine Cx43 mutants. Mutants were labeled with one donor (chelated Tb^{3+})-labeled and one or more fluorescent acceptor-labeled monomers, and distances between donor-acceptor probes were calculated from sensitized acceptor emission lifetimes. The distances allowed for the assignment of M2 (~45 Å) and M3 (~41 Å) as pore-lining, and M1 (~57 Å) and M4 (~60 Å) as peripheral helices. On the extracellular side (narrower side of the pore), the distances were ~23 and ~40 Å, for M2 and M3 residues, respectively. The shorter M2 extracellular-side distance is evidence of tilting and suggests that M2 is helix C, the primary pore-lining helix. Single-Cys mutants of M1, M2 and M4 (8 per helix) were labeled with BADAN, a probe that displays emission maxima at longer wavelengths in hydrophilic environments. BADAN emission peaked at $\geq$ 480 nm in five of the M2 residues studied, none of the M1 and only one M4 residue position (probably exposed to the cytoplasm). From these and previous results, we built a new GJH model with the following helix assignment: M1 = A, M2 = C, M3 = B and M4 = D. This work was supported in part by NIH grants DC007150, GM068586 and GM79629, American Heart Association, Texas Affiliate grant 0755002Y, and Texas Advanced Research Program grant 010674-0046-2007.

1448-Pos Board B292

Bridging Cadherin-mediated Cell Adhesion to Multicellular Pattern Formation by Multiscale Modeling and Simulation

Yinghao Wu, Barry Honig.
Columbia University, New York, NY, USA.

The difficulty to study the cadherin-mediated cell adhesion lies in the complexity from cadherin binding specificity to multi-cellular pattern formation. Cadherins are the main adhesion molecules on the cell membrane to hold cells together. They play important roles in many biological processes, such as cell sorting during embryonic development, acting as tumor-suppressors and also mediating cell signaling. Cadherin binding specificities have been shown to be primarily homophilic, but can be more promiscuous. On the other hand, cell-cell adhesion specificity is not simply correlated with molecular-binding specificity within the cadherin family. It has been suggested that cellular binding specificity also arises from differences in overall cadherin cell surface concentration. In order to understand how these different factors lead to various multi-cellular pattern formation results, we present a computational strategy to model the relation between cadherin binding and cell adhesion in multiscale. Three levels of simulation schemes in different resolutions are constructed to model the multiple cellular system, cell membrane interface and cadherin molecular binding, respectively. Results generated from higher level of simulation are used as input parameters for the simulation in lower level, which combine different modeling into a comprehensive and hierarchic computational strategy. Results from different experimental methods can further be